A&A 578, A109 (2015)
DOI: 10.1051/0004-6361/201526130

Astronomy & Astrophysics

Surface abundances of ON stars⋆,⋆⋆,⋆⋆⋆

F. Martins[1], S. Simón-Díaz[2,3], A. Palacios[1], I. Howarth[4], C. Georgy[5], N. R. Walborn[6], J.-C. Bouret[7], and R. Barbá[8]

[1] LUPM, Université de Montpellier, CNRS, place Eugène Bataillon, 34095 Montpellier, France
e-mail: fabrice.martins@univ-montp2.fr
[2] Instituto de Astrofísica de Canarias, 38200 La Laguna, Tenerife, Spain
[3] Departamento de Astrofísica, Universidad de La Laguna, 38205 La Laguna, Tenerife, Spain
[4] Department of Physics & Astronomy, University College London, Gower St., London WC1E 6BT, UK
[5] Astrophysics group, EPSAM, Keele University, Lennard-Jones Labs, Keele, ST5 5BG, UK
[6] Space Telescope Science Institute, 3700 San Martin Drive, Baltimore, MD, 21218, USA
[7] Aix Marseille Université, CNRS, LAM (Laboratoire d'Astrophysique de Marseille) UMR 7326, 13388 Marseille, France
[8] Departamento de Física y Astronomía, Universidad de La Serena, Cisternas 1200 N, La Serena, Chile

Received 18 March 2015 / Accepted 16 April 2015

ABSTRACT

Context. Massive stars burn hydrogen through the CNO cycle during most of their evolution. When mixing is efficient or when mass transfer in binary systems occurs, chemically processed material is observed at the surface of O and B stars.
Aims. ON stars show stronger lines of nitrogen than morphologically normal counterparts. Whether this corresponds to the presence of material processed through the CNO cycle is not known. Our goal is to answer this question.
Methods. We performed a spectroscopic analysis of a sample of ON stars with atmosphere models. We determined the fundamental parameters as well as the He, C, N, and O surface abundances. We also measured the projected rotational velocities. We compared the properties of the ON stars to those of normal O stars.
Results. We show that ON stars are usually rich in helium. Their CNO surface abundances are fully consistent with predictions of nucleosynthesis. ON stars are more chemically evolved and rotate – on average – faster than normal O stars. Evolutionary models including rotation cannot account for the extreme enrichment observed among ON main sequence stars. Some ON stars are members of binary systems, but others are single stars as indicated by stable radial velocities. Mass transfer is therefore not a simple explanation for the observed chemical properties.
Conclusions. We conclude that ON stars show extreme chemical enrichment at their surface, consistent with nucleosynthesis through the CNO cycle. Its origin is not clear at present.

Key words. stars: massive – stars: abundances – stars: evolution – stars: atmospheres

1. Introduction

Massive stars are born as O and B dwarfs on the main sequence. They subsequently evolve into supergiants of various types (blue, yellow, red) as their effective temperature decreases and their radius increases. Some stars may evolve back and forth between these types of supergiants owing to as-yet poorly-known physical mechanisms (e.g., Georgy et al. 2014). Above about 25 $M_{\odot}$ (at solar metallicity), these stars develop strong winds after the supergiant phase, becoming nitrogen- or carbon-rich Wolf-Rayet stars (WN, WC; e.g., Crowther 2007). The different types of Wolf-Rayet star reflect the different compositions of their surface material: WN stars show nitrogen enrichments and carbon depletions, while WC stars are hydrogen-free and have a high fraction of carbon in their atmospheres.

These chemical properties are direct consequences of different evolutionary states. Massive stars burn hydrogen to helium through the partial or complete CNO cycling (depending on the temperature). In equilibrium, most of the nuclei in the CNO cycle are in the form of nitrogen; consequently, nucleosynthesis in massive stars produces an excess of nitrogen and a depletion of carbon and oxygen. If mixing processes are efficient, part of this processed material can be brought to the surface, and thus be detected spectroscopically. WN stars show the typical chemical patterns of CNO burning; in subsequent evolutionary phases, helium burns to carbon, accounting for the chemical appearance of WC stars.

The CNO cycle proceeds in the cores of massive stars as long as hydrogen is available (i.e., during the main sequence). We therefore expect massive stars to become increasingly nitrogen rich as well as carbon and oxygen poor as they evolve off the zero-age main sequence.

⋆ Based on observations obtained 1) at the Anglo-Australian Telescope; 2) at the Canada-France-Hawaii Telescope (CFHT), which is operated by the National Research Council (NRC) of Canada, the Institut National des Science de l'Univers of the Centre National de la Recherche Scientifique (CNRS) of France, and the University of Hawaii; 3) at the ESO/La Silla Observatory under programs 081.D-2008, 083.D-0589, 086.D-0997; 4) the Nordic Optical Telescope, operated on the island of La Palma jointly by Denmark, Finland, Iceland, Norway, and Sweden, in the Spanish Observatorio del Roque de los Muchachos of the Instituto de Astrofísica de Canarias; 5) the *Mercator* Telescope, operated on the island of La Palma by the Flemish Community at the Spanish Observatorio del Roque de los Muchachos of the Instituto de Astrofísica de Canarias.

⋆⋆ Appendices are available in electronic form at http://www.aanda.org

⋆⋆⋆ The reduced spectra are only available at the CDS via anonymous ftp to cdsarc.u-strasbg.fr (130.79.128.5) or via http://cdsarc.u-strasbg.fr/viz-bin/qcat?J/A+A/578/A109

Rotation is a powerful way of triggering mixing mechanisms in massive stars (Maeder & Meynet 2000; Langer 2012), and evolutionary calculations of rotating stars show that the surface composition of OB stars can be modified by CNO-processed material, even during early evolutionary phases (Brott et al. 2011; Ekström et al. 2012; Chieffi & Limongi 2013). The degree of enrichment depends on several parameters: rotation speed, metallicity, initial mass, and magnetic field.

Observationally, the predictions of stellar-evolution models incorporating rotation have been partly confirmed. Hunter et al. (2008, 2009) show that the majority of the B stars they studied in the Galaxy, Large and Small Magellanic Clouds exhibit nitrogen enrichments as predicted by rotating models, although a non-negligible fraction (20 to 40%) were found to be more enriched than expected for their rotation speed. Przybilla et al. (2010) and Maeder et al. (2014) demonstrate that B stars show surface CNO patterns consistent with the expectations of nucleosynthesis, and Martins et al. (2015) reached similar conclusions for a large sample of Galactic single O stars (see also Bouret et al. 2012, 2013).

Surface abundances can also be modified by mass transfer in binary systems. If the binary separation is small, the more massive component fills its Roche lobe first, because of its faster evolution, and may dump processed material onto the surface of the secondary (Langer et al. 2008). The primary may subsequently explode as supernova, which will either disrupt the system, leaving the chemically-contaminated secondary as a single star, or produce a binary system with a high-mass star and a compact object. During the mass-transfer process, the primary may also transfer angular momentum to the secondary, which is therefore spun up (Wellstein et al. 2001; Petrovic et al. 2005). The faster rotation can trigger additional mixing of the CNO material produced in the secondary's core, contributing further to the modification of surface abundances. Even in the absence of mass transfer, the rotation of binary components may be affected by tidal interactions with consequences for mixing.

Surface abundances are therefore a key to understanding the evolution of single and binary massive stars. Walborn (1970, 1971, 1976) reported the existence of O and B stars with peculiar CNO spectra: the OBN and OBC stars (see also Walborn et al. 2004). In the former, lines of nitrogen (especially N III $\lambda\lambda$4630–4640) are much stronger than in normal OB stars, while they are weaker in the latter. At the same time, C III λ4650 is weak in OBN stars. Most ON stars have a spectral type between O8.5 and O9.7 – where C III and N III lines are easily observed – but some are also found at spectral type O2, based on the morphology of N IV and O IV lines (Walborn et al. 2004). Lester (1973) studied the ON star HD 201345 and concluded that its spectroscopic appearance was due to the presence of CNO-processed material on its surface. Schönberner et al. (1988) studied three ON stars together with two normal O stars and concluded that the ON stars were helium-rich and showed clear signs of CNO processing at their surfaces. Similar conclusions were reached by Villamariz et al. (2002) for the ON star HD 191423. Smith & Howarth (1994) determined the helium abundance of one OC, one normal O, and one ON star. They found an increasing ratio He/H along the OC/O/ON sequence, confirming the suggestion of Walborn (1976) that the OBN and OBC stars represent different degrees of chemical evolution of OB stars. Howarth & Smith (2001) studied the distribution of rotational velocities of ON stars and concluded that, on average, they rotate faster than normal stars, supporting the hypothesis that rotational mixing could account for their anomalous surface abundances (see also Schönberner et al. 1988). Bolton & Rogers (1978) investigated the binary frequency of OBN/OBC stars (see also Boyajian et al. 2005). They found that most OBN stars show radial-velocity variations (with some binary systems clearly identified), while OBC stars seem to be constant.

While these earlier investigations have provided evidence of CNO processing, to date quantitative spectroscopic analyses have focused on helium (Schönberner et al. 1988; Smith & Howarth 1994; Villamariz et al. 2002), employing relatively simple model atmospheres. Determinations of CNO abundances have relied on equivalent-width measurements and curve-of-growth analyses (Schönberner et al. 1988; Villamariz et al. 2002). Consequently, the status of OBN/OBC stars remains unclear, and the origins of the chemical-abundance peculiarities observed at their surfaces are not fully understood: for example, what are the relative roles of rotation and binarity? To progress in understanding OBN stars, we conducted the first quantitative analysis of the helium and CNO abundances of a significant sample of ON stars, using modern non-LTE/line-blanketed atmosphere models. Section 2 of the paper presents the sample and the observational material. The analysis methods are described in Sect. 3 and the results in Sect. 4. These results are discussed in Sect. 5 and our conclusions given in Sect. 6.

2. Observations and sample

The most complete catalog of Galactic late-type ON stars known to date is provided by Walborn et al. (2011). It contains 13 stars: four dwarfs or subgiants, seven giants, and two supergiants[1]. In the present study, we consider twelve stars from this sample. We excluded the ON9.7 II–III(n) star HD 89137 because it is a double-lined spectroscopic binary, and the available data are not sufficient to separate the two components unambiguously.

The spectroscopic data were collected from a number of archives and unpublished material, with the sources and dates of observation listed in Table 1. We give a brief description of each dataset below.

- AAT data were acquired at the 3.9-m Anglo-Australian Telescope with the University College London Echelle Spectrograph (UCLES) and a 31.6 line mm^{-1} grating. Observations were made at several spectrograph settings in order to obtain near-continuous wavelength coverage ~3650–7000 Å at a resolving power $R \simeq 23\,000$, and signal-to-noise levels are $\gtrsim$100 throughout.
- The IACOB spectroscopic database (Simón-Díaz et al. 2011) includes multi-epoch observations for seven of the stars listed in Table 1. The observations, obtained with the FIbre-fed Echelle Spectrograph (FIES, Telting et al. 2014) attached to the 2.5 m Nordic Optical Telescope (NOT), cover the spectral range 3700–7300 Å with $R = 46\,000$. Data reduction was performed with FIEStool[2] and the normalization of the spectra using own procedures developed in IDL.
- Spectra of four targets were extracted from the ESO/FEROS archive. These data were obtained in the context of the OWN project (Barbá et al. 2010, 2014). They have a resolving power of 48 000 and were reduced by the fully automated pipeline distributed by ESO.

[1] Walborn et al. (2011) explicitly exclude two other stars. The first, BD+36 4063, is an O9.7 Iab supergiant (Mathys 1989), known to be a spectroscopic binary (Williams et al. 2009). The second, HD 105056, is classified as ON9.7 Iae (e.g., Maíz-Apellániz et al. 2004), but it may be a lower mass, post-AGB object (Walborn et al. 2011).

[2] http://www.not.iac.es/instruments/fies/fiestool/

Table 1. Observational information.

Star	ST	Instrument	Date of observation
HD 12323	ON9.2 V	FIES	08 Sep. 2011
HD 13268	ON9.5 IIIn	FIES	average
HD 14633	ON8.5 V	ESPaDOnS	09 Oct. 2009
HD 48279	ON8.5 V	FIES	average
HD 91651	ON9.5 IIIn	FEROS	05 May 2009
HD 102415	ON9 IIInn	FEROS	10 Jun. 2008
HD 117490	ON9.5 IInn	FEROS	14 May 2008
HD 123008	ON9.2 Iab	UCLES	22 Jun 1992
HD 150574	ON9 III(n)	FEROS	10 Jun. 2008
HD 191423	ON9 II-IInn	ELODIE	29 Aug. 2004
HD 191781	ON9.7 Iab	UCLES	14 Aug. 1995
HD 201345	ON9.2 IV	ESPaDOnS	26 Jul. 2010

Notes. Spectral types are from Sota et al. (2011, 2014).

- HD 191423 was observed with the Elodie Spectrograph, mounted on the 1.93-m telescope at the Observatoire de Haute-Provence (OHP). The resolving power is 42 000 and the wavelength coverage 3895−6815 Å. Exposure times were chosen to ensure a signal-to-noise ratio of at least 100 at 5200 Å. Reduction was done using the standard reduction pipeline described in Baranne et al. (1996).
- For HD 14633 and HD 201345, spectra were acquired with the ESPaDOnS spectropolarimeter mounted on the Canada–France–Hawaii Telescope. The resolving power is 65 000, and the wavelength coverage is 3700−10 500 Å. Data was reduced with the automated procedure *Libre Esprit*; a full description of the data is given by Wade et al. (2015).

Table 1 lists the observational data used for the spectroscopic analysis. Additional data are described in Table A.1 and are discussed in Sect. 5.3.

3. Modeling and spectroscopic analysis

We used the atmosphere code CMFGEN to analyze the surface properties of the ON stars. A full description of CMFGEN can be found in Hillier & Miller (1998). In a nutshell, CMFGEN solves the radiative transfer and statistical equilibrium equations in the comoving frame, leading to non-LTE models. The temperature structure is set from the radiative-equilibrium constraint. Spherical geometry is adopted to take extension due to the strong winds of O stars into account. The density structure is computed from mass conservation, and the velocity structure is constructed from a pseudo-photospheric structure connected to a β-velocity law. The photospheric structure is obtained from a few iterations of the hydrodynamical solution in which the radiative force computed from the level populations and atomic data is included. The final synthetic spectrum is obtained from a formal solution of the radiative transfer equation.

The synthetic spectra are subsequently compared to observations to determine the stellar parameters. In practice, we proceeded as follows:

- *Rotation and macroturbulence:* we used the Fourier-transform method (Gray 1976) to determine V sin i, the projected equatorial rotational velocity. We relied on O III λ5592 when possible; otherwise, we used He I λ4920. We subsequently estimated the expected $T_{\rm eff}$ and log g from the target's spectral type, using the calibration of Martins et al. (2005), and selected a corresponding synthetic spectrum form our database of models. We convolved this spectrum with a rotational profile (adopting V sin i from the previous step) and performed an additional convolution by a radial–tangential profile (parameterized by a velocity $\upsilon_{\rm mac}$) to take macroturbulence into account (Simón-Díaz & Herrero 2014). We varied $\upsilon_{\rm mac}$ until a good match was obtained to the observed spectrum (especially around 4100 Å, 4700 Å and 4900 Å). Uncertainties on V sin i and $\upsilon_{\rm mac}$ are ∼10 and 20 km s^{-1} respectively.
- *Effective temperature:* we relied on the traditional ionization-balance method to constrain $T_{\rm eff}$. We used the helium lines He I λ4026, He II λ4200, He I λ4388, He I λ4471, He II λ4542, He I λ4712, He I λ4920, He I λ5016, and He II λ5412. We found that when He II λ4542 was perfectly matched, He II λ4200 was usually slightly too strong and He II λ5412 slightly too weak. This is partly attributed to the échelle nature of most of our spectra and thus to uncertain normalization. As a consequence, effective temperatures are determined within about ±1500 K.
- *Surface gravity:* the wings of Balmer lines were used to determine log g, with a typical uncertainty of ∼0.15 dex.

Since our principal focus is on surface parameters, we did not try to reproduce the details of emission lines likely to be formed in the wind (particularly He II λ4686, Hα); instead, we simply adopted combinations of terminal velocity and mass-loss rate that give a reasonable fit to these features in each star, with the wind-acceleration parameter β fixed at 1.0. Luminosities were adopted from the calibration given by Martins et al. (2005). Instrumental broadening was negligible given the high resolution of the observed spectra and the generally large rotational broadening, and our final synthetic spectra were simply convolved by rotational and radial-tangential profiles (see above).

For determining surface abundances, we proceeded as in Martins et al. (2015). For a given $T_{\rm eff}$ and log g, we ran models with different He, C, N, and O abundances. We identified the cleanest lines of each element in the observed spectrum, and performed a χ^2 analysis by combining all selected features. The computed χ^2 values were renormalized to a minimum value of 1.0, with the best-fit abundance taken to correspond to this minimum and 1σ uncertainties defined by $\chi^2 = 2.0$.

For helium, we utilized from seven to ten lines selected from He I λ4026, He II λ4200, He I λ4388, He I λ4471, He II λ4542, He I λ4713, He I λ4920, He I λ5016, He II λ5412, and He I λ6680. Figure 1 shows an example of He/H determination, illustrated by HD 48279. An abundance greater than 0.1 (by number) is clearly favored, simply by inspection. The quantitative analysis re-establishes that He/H = 0.16 ± 0.05 reproduces the set of helium lines best.

Our primary carbon-abundance diagnostic was C III λ4070. For a few stars, C III λ4163, C III λ4188, and C II λ4267 could also be used. We did not use C III λ4650 because of its sensitivity to winds, to metallicity, and to uncertainties in the atomic data (Martins & Hillier 2012). In most cases, we could only obtain an upper limit on C/H because C III λ4070 is the only useful carbon line that could be detected and is rather weak. Difficulties in normalizing the spectra resulting from the presence of nearby Hδ further undermine any attempt to put a tighter constraint on C/H. Figure 2 shows an example of C/H determination, for HD 117490. In this case a conservative upper limit on C/H of 3×10^{-5} is adopted.

The principal nitrogen-abundance indicator was the N III 4510−4535 Å complex of lines. Occasionally, other indicators were added: N II λ3995, N II λ4004, N III λ4044,

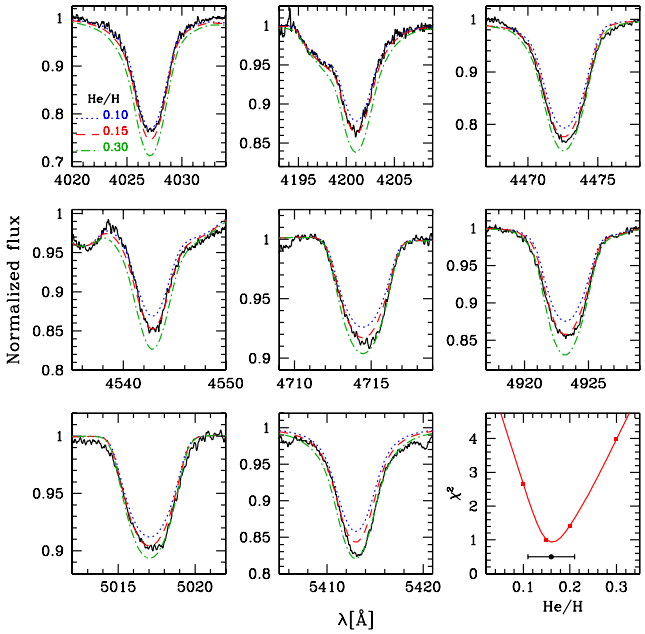

Fig. 1. Determination of the ratio He/H for HD 48279. Observed He I and He II lines are shown by the black solid line. The blue dotted (red dashed; green dot-dashed) lines are models with He/H = 0.10 (0.15; 0.30). The *lower right panel* shows the χ^2 results from the quantitative analysis, from which one determines He/H = 0.16 ± 0.05.

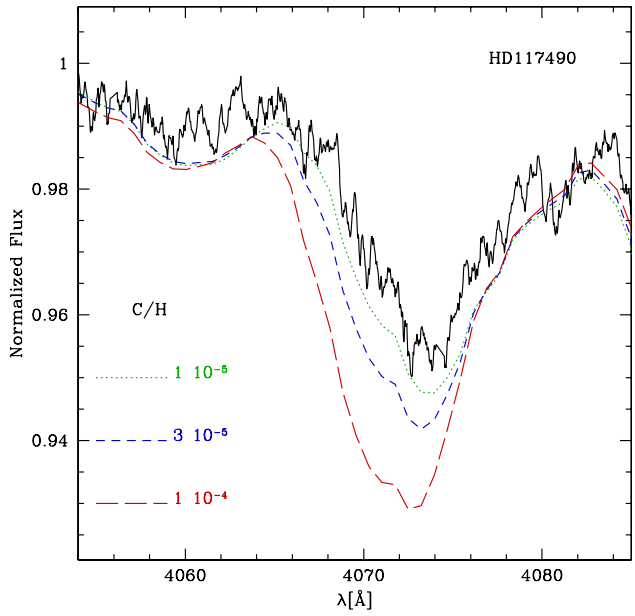

Fig. 2. Observed C III 4070 line of HD 117490 (black solid line), together with models with different C/H values (colored interrupted lines).

N II λ4447, N II λ4607, N II λ5001, N II λ5005, N II λ5011, N II λ5676, and N II λ5680. Finally, O III λ5592 was adopted as the main oxygen-abundance indicator. In some stars, we could also make use of O II λ3913, O II λ3963, O II λ4277-78, O II λ4318, O II λ4368, O II λ4416-18, O II λ4603, and O II λ4611. Compared to normal O stars, fewer useful lines are generally available to determine surface abundances because the ON stars typically have relatively high V sin i values (Howarth & Smith 2001); as a result, weak metallic lines are too broad to be readily detected. Lines from two ionization states are usually taken into account in the abundance determination, so that the error bars include uncertainties related to flawed N and O ionization balances. At the same time, by performing the abundance determination on an ensemble of lines, we minimize uncertainties related to the formation or physics of individual lines (see Fig. 1 in Martins et al. 2015).

We adopted a photospheric microturbulent velocity of 10 km s^{-1} in our synthetic spectra[3]. A higher value would tend to reduce the derived abundances, especially of helium (McErlean et al. 1998; Villamariz & Herrero 2000; Howarth & Smith 2001). Using HD 191423 as a test case, we find that increasing the microturbulence to 20 km s^{-1} leads to a reduction of 0.05 in the inferred He/H ratio.

As a check on our results, we performed a separate analysis of our sample using the IACOB-GBAT package (Simón-Díaz et al. 2011; Sabín-Sanjulián et al. 2014), which uses a χ^2-fitting algorithm coupled to a large, precomputed grid of FASTWIND models (Santolaya-Rey et al. 1997; Puls et al. 2005). This completely independent approach allows the determination of $T_{\rm eff}$, $\log g$, V sin i, $v_{\rm mac}$, and He/H. The results turned out to be in excellent agreement with the CMFGEN analyses, within the respective error bars, lending strong support to our quantitative results.

4. Results

The results of the spectroscopic analysis are summarized in Table 2, and the best-fit models are compared to the observed spectra in Figs. B.1–B.12. We emphasize that the numerical results listed in Table 2 should be viewed as "surface average" values. Many of the sample stars have high rotational velocities, which can affect their shapes and create surface gradients in the physical parameters (e.g., Howarth & Smith 2001; Palate et al. 2013). For HD 191423, the fastest rotator of the sample, rotational broadening is so large that normalization of the echelle spectra was extremely difficult, and carbon and oxygen abundances could not be determined.

Table 2 shows that most ON stars are rich in helium. Smith & Howarth (1994) performed a helium-abundance determination for HD 123008 and obtained He/H = 0.20 ± 0.05, in good agreement with our estimate. Howarth & Smith (2001) determined He/H in HD 191423 using simple non-LTE models without line-blanketing but with a better treatment of 2D effects than our approach. They obtained He/H = 0.23 ± 0.04, in very good agreement with our value. The relatively large helium enrichment of most ON stars indicates a peculiar chemical history compared to normal OB stars, which do not systematically show values of He/H higher than 0.1 (e.g. Mokiem et al. 2007).

Figure 3 shows the surface gravity as a function of effective temperature in our sample. "Geneva" evolutionary tracks from Ekström et al. (2012) are overplotted. We see that the ON stars follow a relatively clear sequence: dwarfs have higher $\log g$ values than giants, while supergiants have the lowest $\log g$, a trend similar to what is found for normal O stars by Martins et al. (2015). Stars classified as ON have a rather narrow range of initial masses: 20–25 $M_\odot$ for the dwarfs and giants and a little over 25 $M_\odot$ for the supergiants, according to the Geneva tracks.

Figure 4 illustrates the N/H ratio (by number) as a function of He/H. The evolutionary models predict a correlation between N/H and He/H that simply results from nucleosynthesis through

[3] Except for HD 123008, for which we found that 20 km s^{-1} gave a better fit of the helium lines.

Table 2. Parameters of the sample stars.

Star	Spectral type	$T_{\rm eff}$ [kK]	log g	log $g_{\rm c}$	V sin i [km s^{-1}]	$v_{\rm mac}$ [km s^{-1}]	He/H	C/H [10^{-4}]	N/H [10^{-4}]	O/H [10^{-4}]
HD 12323	ON9.2 V	33.5	4.00	4.01	130	–	$0.16^{+0.10}_{-0.06}$	<0.3	$3.5^{+2.7}_{-1.8}$	$2.5^{+2.3}_{-1.6}$
HD 13268	ON9.5 IIIn	32	3.50	3.63	310	–	0.20 ± 0.10	<0.5	$5.0^{+2.8}_{-2.0}$	$3.1^{+2.5}_{-1.4}$
HD 14633	ON8.5 V	34	3.80	3.81	100	120	$0.13^{+0.08}_{-0.04}$	<0.3	$5.2^{+5.0}_{-2.5}$	$1.7^{+0.9}_{-0.8}$
HD 48279	ON8.5 V	34.5	3.80	3.82	137	50	0.16 ± 0.05	$0.65^{+0.20}_{-0.20}$	$4.6^{+3.2}_{-2.0}$	$4.3^{+2.0}_{-2.3}$
HD 91651	ON9.5 IIIn	31	3.50	3.62	310	–	$0.14^{+0.08}_{-0.05}$	<0.5	$5.4^{+1.6}_{-1.1}$	$2.3^{+1.9}_{-1.4}$
HD 102415	ON9 IIInn	31	3.50	3.70	376	–	0.21 ± 0.10	<0.6	$7.6^{+4.2}_{-3.6}$	<3.0
HD 117490	ON9.5 IIInn	30.5	3.50	3.66	375	–	$0.16^{+0.09}_{-0.05}$	<0.3	$7.6^{+2.9}_{-2.6}$	$2.5^{+2.6}_{-2.0}$
HD 123008	ON9.2 Iab	30	3.10	3.10	37	100	$0.21^{+0.11}_{-0.07}$	$0.22^{+0.21}_{-0.18}$	$13.5^{+6.7}_{-3.6}$	$4.8^{+2.1}_{-2.1}$
HD 150574	ON9 III(n)	31	3.40	3.49	240	–	0.23 ± 0.06	<0.5	>10.0	$6.0^{+2.9}_{-2.3}$
HD 191423	ON9 II-IIInn	31.5	3.50	3.72	445	–	0.25 ± 0.08	–	>5.0	–
HD 191781	ON9.7 Iab	28	3.10	3.12	107	70	$0.25^{+0.2}_{-0.1}$	<0.5	$7.3^{+7.3}_{-5.0}$	$3.1^{+0.8}_{-0.8}$
HD 201345	ON9.2 IV	34	4.00	4.01	95	60	0.1	<0.4	$4.0^{+2.2}_{-1.3}$	$3.6^{+2.7}_{-2.2}$

Notes. Uncertainties on $T_{\rm eff}$, log g, V sin i and $v_{\rm mac}$ are ~1.5 kK, 0.15 dex, 10, and 20 km s^{-1} respectively. log $g_{\rm c}$ is the surface gravity corrected for centrifugal acceleration. Abundances are number ratios.

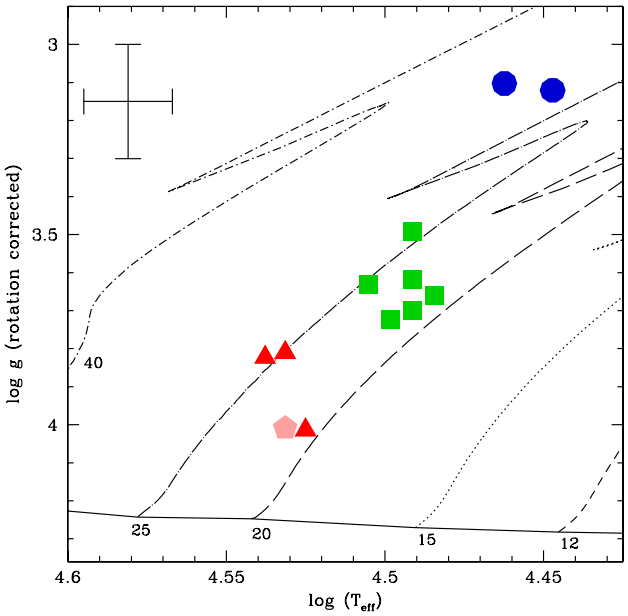

Fig. 3. log g−log($T_{\rm eff}$) diagram for the sample stars. Triangles (pentagons, squares, circles) are for luminosity class V (IV, III, I) stars. Typical uncertainties are shown in the upper left corner. Evolutionary tracks including rotation, from Ekström et al. (2012), are overplotted and labeled by ZAMS masses.

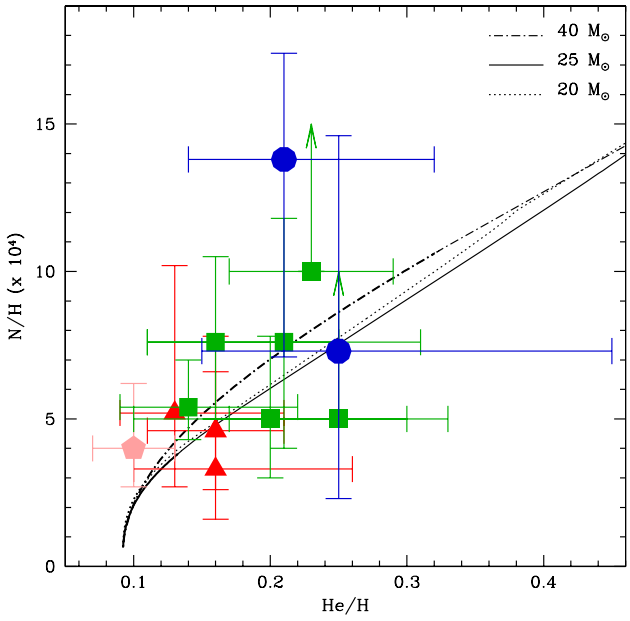

Fig. 4. N/H as a function of He/H for the ON stars. The abundance ratios are by number. Symbols have the same meaning as in Fig. 3. The evolutionary tracks including rotation of Ekström et al. (2012) are overplotted. The bold part corresponds to the main sequence (central hydrogen mass fraction >0).

the CNO cycle: the higher the helium content, the higher the nitrogen abundance. Figure 4 shows a possible trend of this kind among the ON stars, but the rather large error bars on the abundance determinations do not allow for a clear-cut conclusion observationally. Most stars appear more enriched than expected from their position in the log g−log($T_{\rm eff}$) diagram.

Figure 5 shows the ratio of the nitrogen-to-carbon surface abundance as a function of surface gravity for the ON stars[4] and for a reference sample of morphologically normal O stars taken from Martins et al. (2015). For the reference sample, only stars with spectral types between O8.5 and O9.7 are considered, corresponding to the spectral-type range of the ON sample. The dwarf, giant, and supergiant stars are well separated in this plane, among both ON and reference groups, which largely reflects the surface-gravity differences between luminosity classes, as is also seen in Fig. 3. The most striking feature of Fig. 5 is the higher log(N/C) ratios found for ON stars for a given luminosity class. The difference amounts to 0.5−1.0 dex or more, since most of the log(N/C) values for ON stars are actually lower limits (due to the upper limits on C/H; Table 2). Another possible trend is that of higher log(N/C) among ON stars as one moves from dwarfs to giants and supergiants. This trend was clearly established for morphologically normal stars by Martins et al. (2015) and also appears to hold for ON stars. This suggests that the physics of chemical mixing follows the same patterns in normal

[4] As discussed previously, only upper limits to C/H are available in most cases.

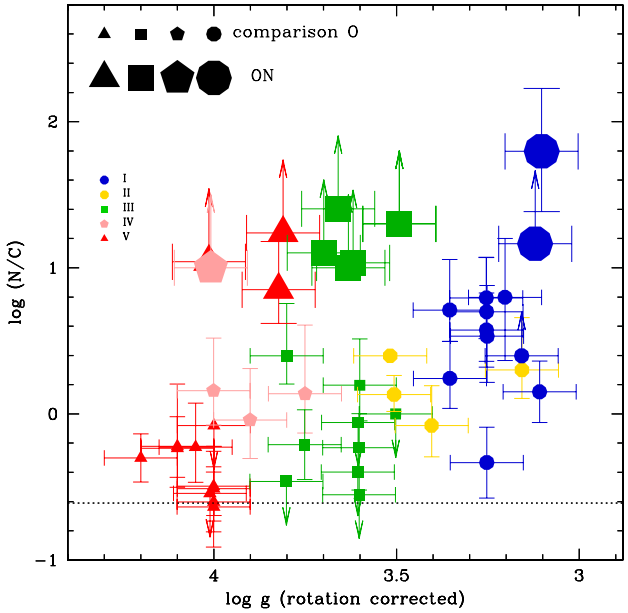

Fig. 5. N/C abundance ratio as a function of surface gravity for the ON stars (large symbols), compared to results for morphologically normal stars with spectral types O8.5–9.7 (small symbols), taken from Martins et al. (2015).

and ON stars, pointing to a common origin for surface chemical enrichment. However, we caution that the trend for ON stars is less clear owing to both the small number of objects and the fact that for most stars, we only have lower limits on log(N/C).

Figure 6 shows the log(N/C) versus log(N/O) diagram. The upper lefthand panel reveals that the ON stars are systematically more enriched than the comparison O stars taken from Martins et al. (2015). They extend the relation between log(N/C) and log(N/O) observed for normal stars to higher abundance ratios and are also located between the limits corresponding to partial CN burning and complete CNO burning. Consequently, the abundance patterns of ON stars are consistent with the predictions of nucleosynthesis through the CNO cycle.

Other panels of Fig. 6 compare results for ON and normal O stars in different luminosity classes. In each case, the ON stars are clearly separated from the comparison stars, indicating that their surface abundances result from a much stronger mixing than experienced by normal stars. Martins et al. (2015) showed that, on average, supergiants are more enriched than giants and dwarfs. We saw in Fig. 5 that this trend may exist among ON stars, too. Figure 6 tends to confirm that there is a sequence of higher enrichment when moving from dwarfs to giants and supergiants, although there is one outlier (HD 14633, a dwarf that appears to be as chemically mixed as the giants).

Figures 5 and 6 show gaps between the distributions of the ON stars and those of the comparison stars, and the reader may wonder whether these are real features. In this context, then supposing that chemical mixing may be due to rotation (and Howarth & Smith 2001 have shown that ON stars rotate on average faster than normal O stars), it is informative to consider the distributions of projected rotational velocities in the two samples. This comparison is performed in Fig. 7; clearly, the stars in the comparison sample are rotating much more slowly on average than those of the ON stars. The median V sin i value for the ON and comparison-O samples are 208.0 and 52.5 km s^{-1}, and a KS test indicates a probability of less than 1% that the two populations are drawn from the same parent distribution.

Figure 7 also includes the V sin i distribution of the IACOB sample studied by Simón-Díaz & Herrero (2014). They provided projected rotational velocities for 199 Galactic O stars, which can be viewed as a reference distribution for O stars in general; the ON stars have higher V sin i values, and our comparison O stars lower ones, than the Simón-Díaz & Herrero reference sample. Potentially, therefore, the very different ranges of V sin i covered by our two samples (ON and comparison) can explain the gap seen in Fig. 6: if rotation leads to a continuous increase in mixing as V sin i increases, and if our two samples are separated well in terms of projected rotational velocity, then a separation into two groups in the log(N/C)–log(N/O) and log(N/C)–log g diagrams is expected.

5. Discussion

5.1. Spectral classification and ON stars

The spectroscopic classification qualifier "N" was developed in the context of late-O and early-B stars, as is illustrated by our sample, which is limited to spectral types between O8.5 and O9.7. Walborn et al. (2004) discovered a related morphological dichotomy in terms of CNO features at the earliest spectral type, O2, where some stars show relatively strong O IV lines and weak N IV lines. The opposite behavior is found in a second group, for which the spectral classification ON2 was therefore created, by analogy to the behavior in late-O stars.

It is important to note that different lines are used when classifying ON2 and late-type ON stars; lines from more highly ionized elements are observed in the former group (O IV, N IV) than in the latter (C III, N III). This, rather than some fundamental difference in surface chemistry, largely accounts for why the "N" qualifier is not assigned to O stars at intermediate spectral types – when moving from O2 to later spectral types, the diagnostic O IV and N IV lines disappear because of ionization effects. On the other side of the classification scheme, the C III and N III lines around 4630–4650 Å, which define the late-type ON category, progressively go into emission at spectral types earlier than O8. In principle, the strength of these emission features could be used in a similar manner to their absorption counterparts in late-type stars, but the strength of the emission in these lines is complicated by wind effects (Rivero González et al. 2011; Martins & Hillier 2012). Interestingly, Walborn et al. (2010) have recently defined the Ofc class, corresponding to stars showing N III λ4630–4640 in emission and C III λ4650 of comparable strength. The difference between Ofc and Of stars may be the equivalent of the ON phenomenon at O2 and late-O spectral types (Of stars having comparatively weaker C lines than Ofc stars).

5.2. Rotation and the ON phenomenon

Fast rotation could explain the strong chemical enrichments that we have found in ON stars, which rotate on average faster than normal O stars (Howarth & Smith 2001, and Sect. 4)[5]. Theoretical predictions indicate that faster rotation leads to stronger mixing (Maeder & Meynet 2000; Langer 2012; Brott et al. 2011; Ekström et al. 2012; Chieffi & Limongi 2013; Georgy et al. 2013a), and thus to the appearance of more-strongly processed material on the surface of OB stars.

[5] We recall that such fast rotation could result from formation processes or may arise through tidal interactions in binary systems (which would not necessarily have experienced mass transfer; Langer et al. 2008).

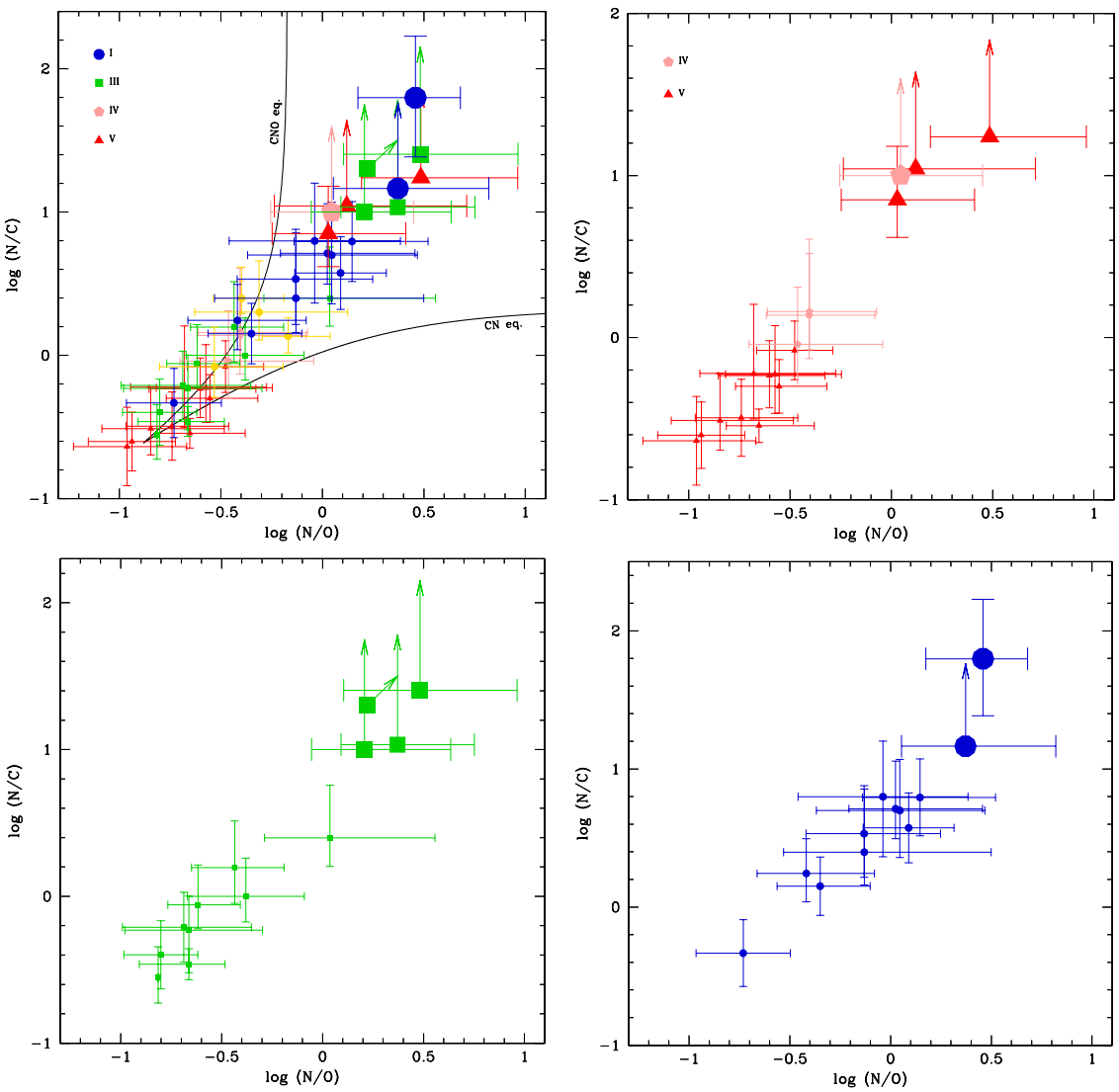

Fig. 6. Distributions of log (N/C) versus log(N/O) for the ON stars (large symbols) and for a comparison set of normal O stars with spectral types O8.5–O9.7 (small symbols) taken from Martins et al. (2015). The *upper left panel* shows the full sample. The *upper right* (*lower left, lower right*) shows the dwarf–subgiant (giant, supergiant) sample. Solid lines in the *upper left panel* show the relations expected for partial CN or complete CNO burning in equilibrium.

Walborn et al. (2004) performed surface-abundance determinations for O2 and ON2 stars and concluded that the latter were more chemically processed than the former. From their positions in the Hertzsprung–Russell diagram, they argue that ON2 stars may be the product of homogeneous evolution, which is usually understood as a consequence of fast rotation (Maeder 1987; Langer 1992).

Figure 8 compares our abundance determinations with several stellar-evolution models, computed for 25 $M_{\odot}$ stars at solar metallicity, from Ekström et al. (2012), Chieffi & Limongi (2013), and a dedicated model computed with the STAREVOL code (Siess 2006; Decressin et al. 2009) for which we implemented the same physical ingredients as in Ekström et al. (2012): core overshooting, mass-loss prescriptions, angular-momentum-transport equation, and turbulent-transport prescriptions. All the models start on the zero-age main sequence with an equatorial surface velocity of 300 km s^{-1} (equivalent to $V \approx 0.4V_{\rm c}$, where $V_{\rm c}$ the critical surface velocity).

All the inferred abundances lie close to the theoretical tracks, which confirms that they broadly follow the predictions of nucleosynthesis and chemical mixing[6]. However, the abundances predicted at the end of the main sequence (i.e., when the hydrogen mass fraction in the core reaches zero) vary significantly between codes, owing to the sensitivity of the mixing efficiency on both the adopted prescriptions for the shear turbulence (vertical shear from Maeder 1997 in Ekström et al. 2012; and from Talon & Zahn 1997 in Chieffi & Limongi 2013) and on the numerical treatment itself. Nevertheless, we see that the ON stars are all located beyond the end of the main sequence in the log(N/C)–log(N/O) plane. While this may be possible for supergiants, the giants and dwarfs are certainly expected to still be core hydrogen burning (see Fig. 3). The surface abundances of ON stars are thus more enriched than predicted by any of the available models, assuming a standard rotation rate on the main sequence.

Scrutiny of 15-$M_{\odot}$ models from Georgy et al. (2013b) suggests that surface enrichment of CNO-cycle products can be increased significantly (by up to a factor of 3 compared to

[6] The STAREVOL calculations were stopped just after the end of the main sequence.

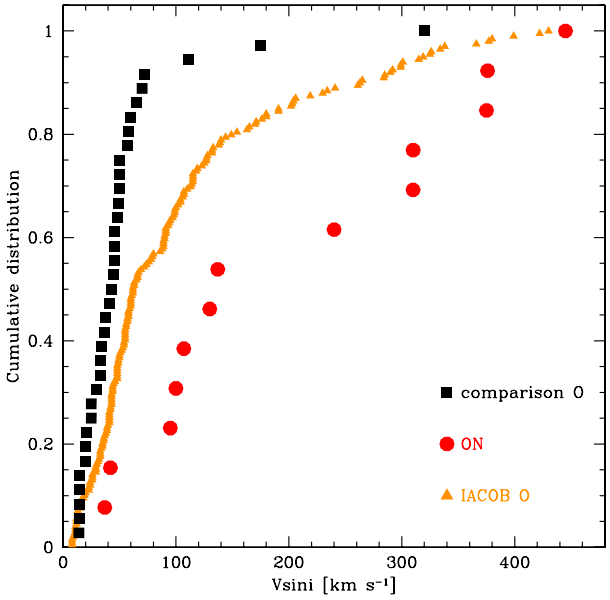

Fig. 7. Cumulative distribution functions of projected rotational velocities for the ON sample (red circles), our comparison sample (black squares), and the IACOB O-star sample (Simón-Díaz & Herrero 2014; orange triangles).

normally rotating stars) through adopting initial rotation rates close to the break-up velocity. It is therefore tempting to speculate that the nitrogen abundances of ON stars can be attributed to the enhanced efficiency of rotational mixing in extremely fast-rotating stars. To test this hypothesis, new 25-$M_{\odot}$ models were computed using the Geneva code, with ratios of initial to critical equatorial velocities, V/V_c, of 0.6 and 0.8 (see Fig. 3). Results are presented in Fig. 9. The lefthand panel shows that increasing the initial rotational velocity leads to a more "upward" evolution (i.e., the effective temperature decreases less at higher velocity). All non-supergiant ON stars are located between the zero-age main sequence and the terminal main sequence, regardless of the initial rotation speed. The middle panel of Fig. 9 shows the corresponding surface abundances; as expected, faster rotation leads to stronger enrichment. At the end of the main sequence, the $V/V_c = 0.8$ model barely reaches the region occupied by the ON stars. However, this happens when $\log g < 3.5$, and the surface enrichment is weaker for the range of surface gravities of non-supergiant ON stars (3.5−4.0). Consequently, evolutionary models with high rotation velocities do not appear to explain the extreme enrichment of ON stars, at least with the current formalism used to treat rotation.

The righthand panel of Fig. 9 shows the effect of adding magnetism to the $V/V_c = 0.6$ model. This models includes the effects of the internal magnetic fields on the mixing of chemicals and angular momentum, according to the Tayler-Spruit dynamo theory (Spruit 2002; Maeder & Meynet 2004). In this framework, internal magnetic fields produces a strong coupling between the core and the surface and considerably increases the internal mixing (e.g., Maeder & Meynet 2005). Significant enrichment, which is consistent with that of ON stars, can be produced while $\log g > 3.5$. However, inspection of the lefthand panel of Fig. 9 reveals that this model produces a blueward evolution and never reaches the position of the ON stars.

Models aside, if rotational mixing is the principal cause of the ON phenomenon, one may wonder why all fast-rotating O stars are not classified as ON. For example, ζ Oph has a projected rotational velocity of about 400 km s^{-1} (e.g., Marcolino et al. 2009), but its spectral type is simply O9.2 IVnn (Sota et al. 2014), where the "nn" qualifier reflects the strong rotational broadening; that is, ζ Oph is not classified as an ON star (see also Howarth & Smith 2001). Villamariz & Herrero (2005) performed a quantitative analysis of its stellar parameters and surface abundances (using equivalent width measurements and the curve-of-growth method). Using more recent atmosphere models than Villamariz & Herrero, Marcolino et al. (2009) refined the $T_{\rm eff}$ and $\log g$ determination. ζ Oph, together with the fast rotators of the sample of (Martins et al. 2015; i.e., stars with $V \sin i > 250$ km s^{-1}) are shown in Fig. 10. The lefthand panel of Fig. 10 demonstrates that the ON stars are more chemically processed than the non-ON fast rotators. The only non-ON fast rotator with a strong enrichment is HD 192281 (O4.5 Vn(f)), the most massive dwarf of the sample, and its enrichment is probably due to its higher mass (see discussion in Martins et al. 2015).

Since chemical enrichment depends not only on rotation but also on metallicity, mass and age, one may wonder if the non-ON fast rotators are less evolved or less massive than the ON stars (supposing their metallicities to be similar since all stars are located in the Galaxy). The righthand panel of Fig. 10 shows that ON and non-ON stars are distributed in the same area of the $\log g$–$T_{\rm eff}$ diagram. Thus, they have similar mass and age ranges. In conclusion, if ON stars appear to rotate faster than normal stars on average, not all fast rotators necessarily display the ON phenomenon. Another mechanism may be required, in addition to rotation, to produce ON stars.

5.3. Binarity and the ON phenomenon

Bolton & Rogers (1978) reported that most of the ON stars known at the time of their study were radial velocity (RV) variables, but OC stars were all RV constant. Walborn et al. (2011) discuss radial-velocity variability and the presence of companions in the most recent ON sample. Of the two O supergiants in our study, HD 123008 is reported to be constant in radial velocity, while HD 191781 may be variable. The variability status of the giants is quite uncertain, with some claims of RV variations, but based on limited numbers of measurements. The nature of the tentative variability observed in the giant sample is also unclear: binarity or wind or photospheric variability? Of the five dwarfs or subgiants, HD 48279 is constant in radial velocity (Mahy et al. 2009), HD 12323 is a single-lined spectroscopic binary (SB1; Bolton & Rogers 1978), HD 14633 an SB1 with a low-mass component and high eccentricity (Boyajian et al. 2005), HD 102415 is reported as "likely variable" by Walborn et al. (2011), and HD 201345 has an unclear status.

Figure 11 provides more information on the line-profile and radial-velocity variations of ten of the ON stars studied in the present paper. The data used to build Fig. 11 are described in Table A.1. We chose He I λ5876 for study, since nearby telluric lines can be checked for wavelength-calibration issues. We confirm that HD 12323 and HD 14633 are SB1, with clear RV variations. HD 48279 is very stable in our data, but do not HD 191423 or HD 201345 show signs of variability. All other stars examined (HD 13268, HD 91651, HD 102415, HD 117490, HD 123008) show some degree of RV variability, the origins of which are unclear (RV modulations, pulsations, wind variability).

The exact position with respect to the binarity among ON star is thus not completely clear. Variations in radial velocities are observed in a large part of the sample, but these are unambiguously attributable to binarity only in the few cases for which an orbital solution can be found (HD 12323, HD 14633)

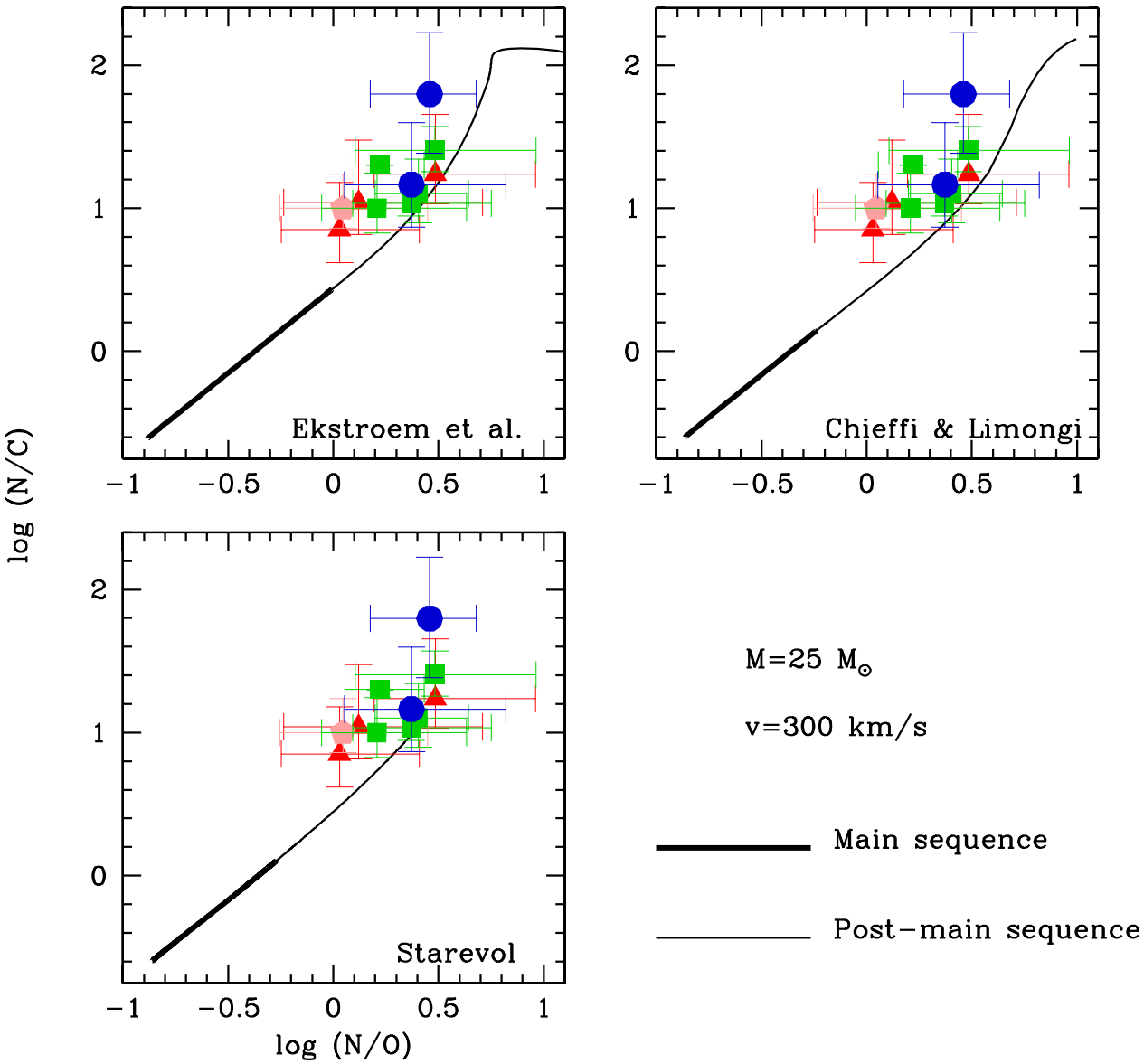

Fig. 8. As in Fig. 6, with evolutionary tracks for a ZAMS mass of 25 $M_{\odot}$, including rotation (with an initial equatorial velocity of about 300 km s^{-1}). Models are from Ekström et al. (2012; *top left*), Chieffi & Limongi (2013; *top right*), and the STAREVOL code (*bottom left*). Thick line sections correspond to core hydrogen burning.

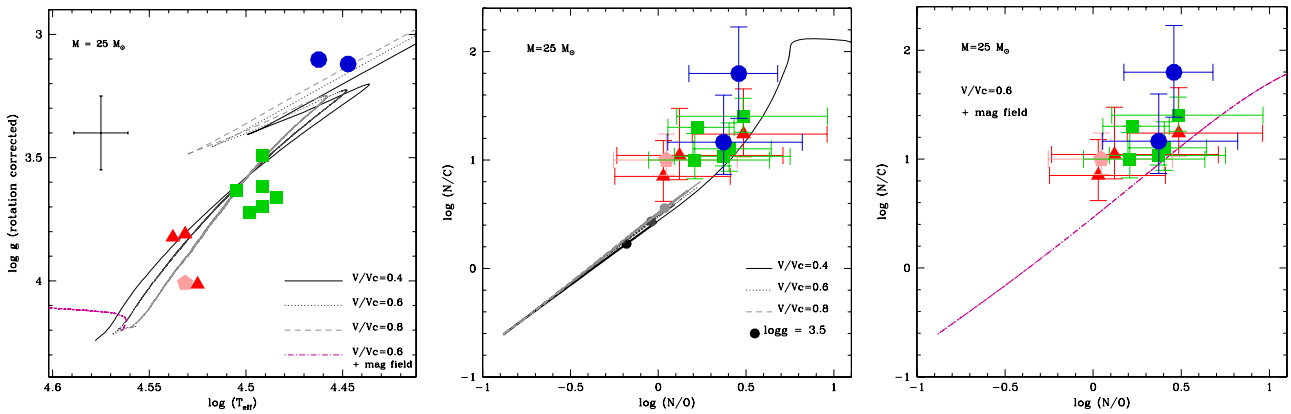

Fig. 9. Effect of rotation on a 25 $M_{\odot}$ evolutionary model. *Left:* log g−log($T_{\rm eff}$) diagram. *Middle:* log(N/C)−log(N/O) diagram for models at different velocities. *Right:* log(N/C)−log(N/O) diagram for a model including magnetic field and $V/V_{\rm c}$ = 0.6. The bold part of the tracks corresponds to the main sequence. Dots in the *middle panel* correspond to a surface log g = 3.5, i.e. the minimum value for dwarfs and giants in the *lefthand panel*; in the *righthand panel*, log g is always higher than 3.5. Models for $V/V_{\rm c}$ = 0.4 are from Ekström et al. (2012). Models for higher velocities have been computed for the present study with the Geneva code until the red supergiant phase.

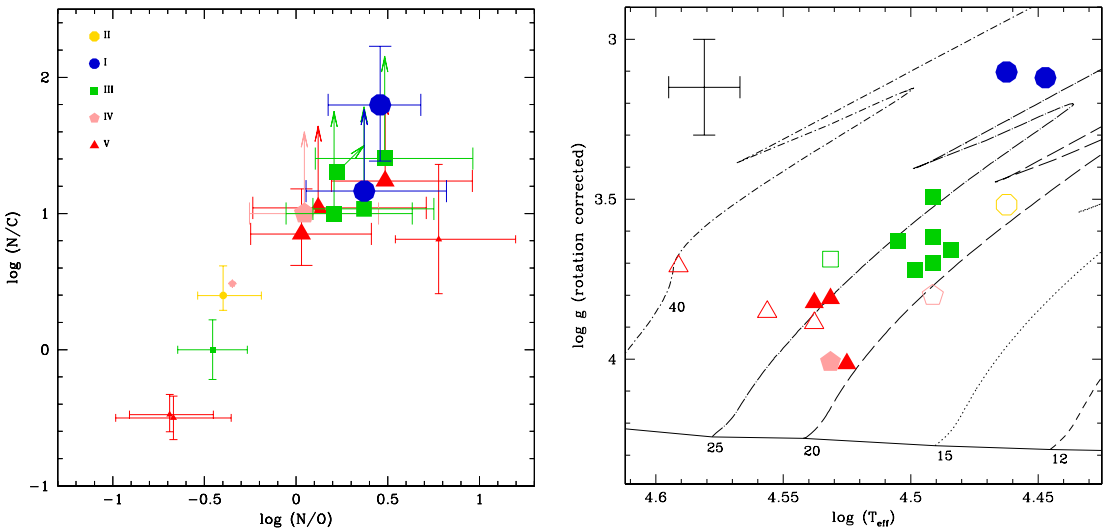

Fig. 10. Comparison between ON and non-ON fast-rotating stars. *Left*: log(N/C) vs. log(N/O) diagram. *Right*: log g–log($T_{\rm eff}$) diagram. Large symbols are ON stars from the present study; open/small symbols are fast rotating stars (V sin i > 250 km s^{-1}) from Martins et al. (2015). The star ζ Oph is also included: effective temperature and surface gravity are from Martins et al. (2015), and surface abundances are from Villamariz & Herrero (2005).

or when an SB2 spectrum is observed (HD 89137). For the majority of the sample stars, radial velocity variations do not have an unambiguous origin (they may be due to binarity or wind or photospheric variability), while a few stars' spectra are consistent with constant radial velocities.

This raises the question of the role of binarity in the strong chemical mixing that we have shown to be a clear-cut characteristic of ON stars. More specifically, one may wonder if mass transfer is responsible for this strong enrichment. In the classical mass-transfer scenario, material processed through nucleosynthesis in the core of a companion is dumped onto what we observe today as an ON star. Stars with an SB1 spectrum may be consistent with this scenario. The secondary may be a low-mass star, possibly a compact object resulting from the evolution and supernova explosion of an initially more massive star than the present-day primary. This initially more massive star could have contaminated the companion that we observe today as chemically enriched before exploding as supernova. The system would have had to stay bound during the supernova phase to account for the SB1 RV curve. A mass-transfer scenario may also be applicable to RV-constant ON stars. These stars could initially have been part of binary systems in which mass transfer occurred before disruption in the supernova phase.

Bolton & Rogers (1978) argued that no sign of current episodes of mass transfer was observed among ON stars, especially dwarfs. Plaskett's star is a famous binary system that is very probably in a post-Roche-lobe overflow phase (Linder et al. 2008) and which shows strong line emission and variability. This is not observed currently among the ON stars we studied in the present paper, indicating that active mass transfer is probably not important among them. HD 48279, which has very similar parameters to the SB1 system HD 14633, does not show RV variations. Both stars are located very close to each other in the log g–$T_{\rm eff}$ diagram (Fig. 3), so their surface chemical enrichment cannot be clearly attributed to mass transfer, given that one is in a binary system and the other apparently is not, although we cannot exclude the possibility that HD 48279 is the result of the merger of two stars, which could explain, at least qualitatively, the strong mixing of CNO material.

However, mass transfer is very probably taking place in the binary BD+36 4063 (not included in our sample). Williams et al. (2009) show that this system contains a ON9.7Ib star with periodic radial-velocity variations. The secondary component is not observed, although for its estimated mass it should be seen in high-resolution spectra. Williams et al. argue that the ON star is currently transferring mass to the companion, surrounding it by a thick disk, thereby preventing the secondary from being detected spectroscopically. In this system, therefore, the ON star is currently the mass donor.

A parallel situation is encountered in the massive SB2 system LZ Cep. Unlike BD+36 4063, the companion in LZ Cep is clearly detected, excluding the presence of a thick circumstellar disk arising from ongoing mass transfer. Mahy et al. (2011) obtained multi-epoch spectroscopy of the system and disentangled the spectra of both components, to which they assigned spectral types of O9 III + ON9.7 V (primary, secondary). Their quantitative analysis of the individual components' spectra showed the secondary to be significantly nitrogen rich and carbon/oxygen poor: log(N/C) (respectively log(N/O)) reaches 1.6 (1.3). The secondary component therefore shows the typical abundance patterns of ON stars, as established in the present study. Mahy et al. (2011) interpret the surface abundances of the secondary as the result of a previous episode of mass transfer in which the secondary was initially the most massive star. The ON star in LZ Cep evolved faster and transferred mass to what was original the secondary (now seen as the primary). In this scenario, the abundance pattern of the ON secondary star is due to the removal of external layers during the mass-transfer phase, thereby exposing internal layers of the star. These internal layers are more chemically mixed and thus show CNO processed material; that is, for LZ Cep (and possibly BD+36 4063) the ON star would have been created because of mass removal and not mass accretion.

Thus, the role of binarity (and mass transfer) in the appearance of the ON phenomenon is not obvious. It is even less clear if we once again consider the fast rotator ζ Oph, which is a runaway (Blaauw 1961; Tetzlaff et al. 2011). Runaways may be produced by dynamical interactions in young, dense clusters or by supernova ejection from a binary system. Dynamical interaction in clusters usually involves at least one binary system (Hut & Bahcall 1983; Hoffer 1983; Hoogerwerf et al. 2001). Consequently, there is a high probability that ζ Oph was part of

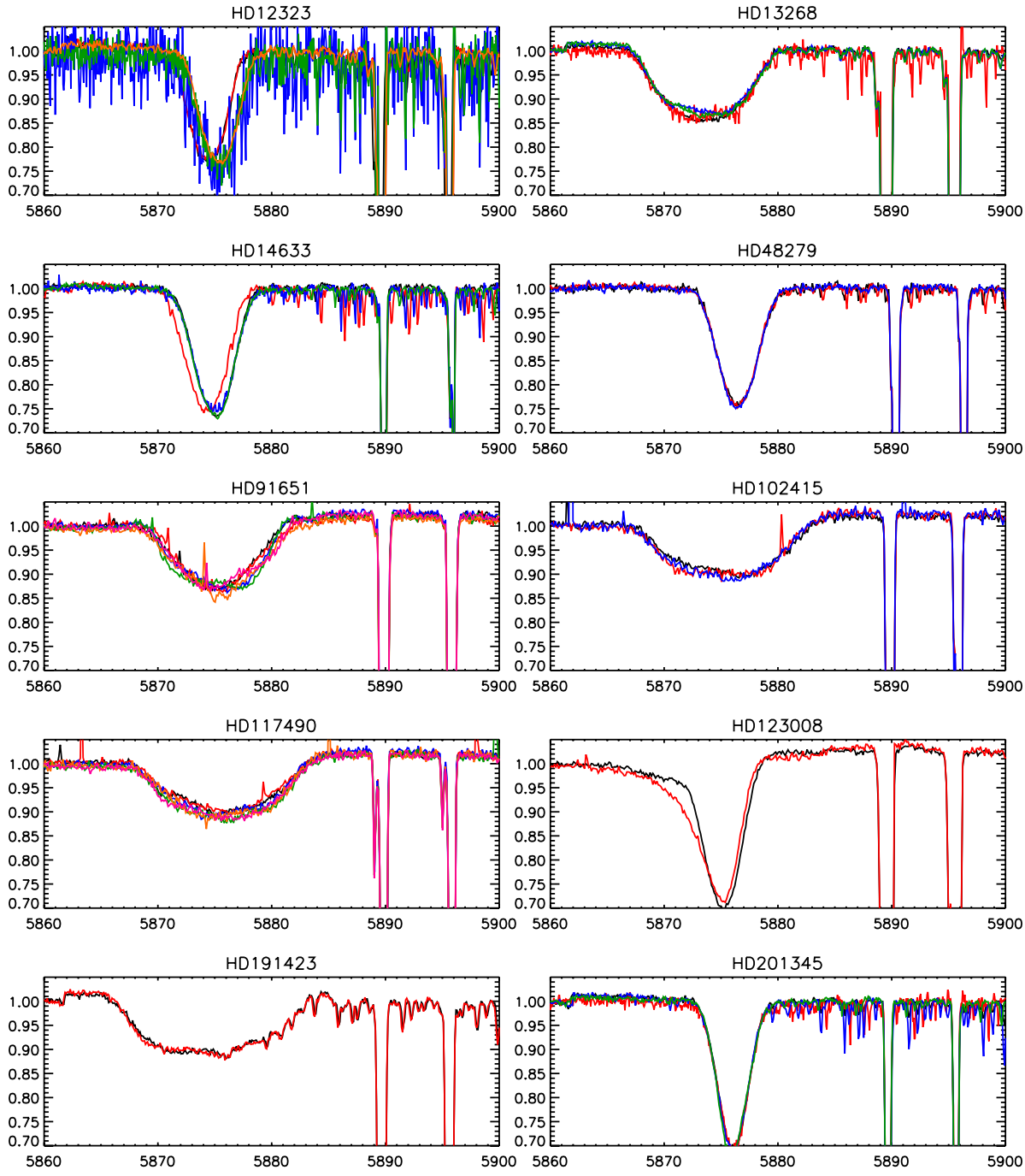

Fig. 11. Variability of ON stars. For each object, a selection of spectra centered on He I λ5876 is shown. The spectra are described in Table A.1.

a binary system at an earlier stage in its evolution; in particular, (Hoogerwerf et al. 2000; see also van Rensbergen et al. 1996) argue that ζ Oph resulted from a supernova kick. Regardless of the evolutionary and dynamical history of this star, it did not reach the level of enrichment seen in ON stars. Consequently, the combination of binarity and fast rotation (possibly acquired through tidal spin-up) does not appear to lead inevitably to the ON phenomenon.

6. Conclusions and final remarks

We performed a spectroscopic analysis of a sample of ON stars using atmosphere models computed with the code CMFGEN. We determined the fundamental parameters and the He, C, N, and O surface abundances, along with projected rotational velocities. The results can be summarized as follows:

- These late-type ON stars have initial masses in the range 20 to 25 $M_{\odot}$, with the two supergiants of the sample being slightly more massive.
- The projected rotational velocities of ON stars are on average higher than those of comparison samples of normal O stars (Martins et al. 2015; Simón-Díaz & Herrero 2014).
- ON stars are chemically enriched; almost all have a helium-to-hydrogen number ratio greater than 0.1. All stars are nitrogen rich, carbon poor, and to a lesser extent, oxygen poor. The surface CNO abundances are consistent with nucleosynthesis predictions.

- ON stars are more chemically mixed than morphologically normal stars of similar spectral types and luminosity classes in the sample of Martins et al. (2015).
- Some ON stars are members of binary systems; some show radial-velocity variations of unclear origin; some are constant in radial velocity.
- Evolutionary models including rotation are not able to reproduce the high degree of chemical mixing observed on the main sequence among ON stars.

From these results, we conclude that ON stars are O stars showing CNO-processed material at their surface; the N/C and N/O ratios we establish are the highest observed so far in O stars. The processed material is the product of nucleosynthesis, but the mechanisms by which it is brought to the surface remains unclear (rotational mixing and binary mass transfer being the prime suspects). ON stars rotate on average faster than normal stars, but fast rotators exist with similar masses and ages that are not ON stars. There are also binary and (presumably) single stars among the ON category, as well as non-ON fast rotators that are (probably) former members of binary systems.

Acknowledgements. We thank John Hillier for making CMFGEN available to the community. F.M. and A.P. thank the Agence Nationale de la Recherche for financial support (grant ANR-11-JS56-0007). S.S.-D. acknowledge funding by the Spanish Ministry of Economy and Competitiveness (MINECO) under the grants AYA2010-21697-C05-01, AYA2012-39364-C02-01, and Severo Ochoa SEV-2011-0187, and by the Canary Islands Government under grant PID2010119. C.G. acknowledges support from the European Research Council under the European Unions Seventh Framework Program (FP/2007-2013)/ERC Grant Agreement No. 306901. R.B. ackowledges support from FONDECYT Regular Project 1140076. STScI is operated by the Association of Universities for Research in Astronomy, Inc., under NASA contract NAS5-26555. We thank an anonymous referee for a timely and positive report.

References

Baranne, A., Queloz, D., Mayor, M., et al. 1996, A&AS, 119, 373
Barbá, R. H., Gamen, R., Arias, J. I., et al. 2010, Rev. Mex. Astron. Astrofis. Conf. Ser., 38, 30
Barbá, R., Gamen, R., Arias, J. I., et al. 2014, Rev. Mex. Astron. Astrofis. Conf. Ser., 44, 148
Blaauw, A. 1961, Bull. Astron. Inst. Netherlands, 15, 265
Bolton, C. T., & Rogers, G. L. 1978, ApJ, 222, 234
Bouret, J.-C., Hillier, D. J., Lanz, T., & Fullerton, A. W. 2012, A&A, 544, A67
Bouret, J.-C., Lanz, T., Martins, F., et al. 2013, A&A, 555, A1
Boyajian, T. S., Beaulieu, T. D., Gies, D. R., et al. 2005, ApJ, 621, 978
Brott, I., de Mink, S. E., Cantiello, M., et al. 2011, A&A, 530, A115
Chieffi, A., & Limongi, M. 2013, ApJ, 764, 21
Crowther, P. A. 2007, ARA&A, 45, 177
Decressin, T., Mathis, S., Palacios, A., et al. 2009, A&A, 495, 271
Ekström, S., Georgy, C., Eggenberger, P., et al. 2012, A&A, 537, A146
Georgy, C., Ekström, S., Eggenberger, P., et al. 2013a, A&A, 558, A103
Georgy, C., Ekström, S., Granada, A., et al. 2013b, A&A, 553, A24
Georgy, C., Saio, H., & Meynet, G. 2014, MNRAS, 439, L6
Gray, D. F. 1976, The observation and analysis of stellar photospheres (Cambridge University Press)
Hillier, D. J., & Miller, D. L. 1998, ApJ, 496, 407
Hoffer, J. B. 1983, AJ, 88, 1420
Hoogerwerf, R., de Bruijne, J. H. J., & de Zeeuw, P. T. 2000, ApJ, 544, L133
Hoogerwerf, R., de Bruijne, J. H. J., & de Zeeuw, P. T. 2001, A&A, 365, 49
Howarth, I. D., & Smith, K. C. 2001, MNRAS, 327, 353
Hunter, I., Brott, I., Lennon, D. J., et al. 2008, ApJ, 676, L29
Hunter, I., Brott, I., Langer, N., et al. 2009, A&A, 496, 841
Hut, P., & Bahcall, J. N. 1983, ApJ, 268, 319
Langer, N. 1992, A&A, 265, L17
Langer, N. 2012, ARA&A, 50, 107
Langer, N., Cantiello, M., Yoon, S.-C., et al. 2008, in IAU Symp. 250, eds. F. Bresolin, P. A. Crowther, & J. Puls, 167
Lester, J. B. 1973, ApJ, 185, 253
Linder, N., Rauw, G., Martins, F., et al. 2008, A&A, 489, 713
Maeder, A. 1987, A&A, 178, 159
Maeder, A. 1997, A&A, 321, 134
Maeder, A., & Meynet, G. 2000, ARA&A, 38, 143
Maeder, A., & Meynet, G. 2004, A&A, 422, 225
Maeder, A., & Meynet, G. 2005, A&A, 440, 1041
Maeder, A., Przybilla, N., Nieva, M.-F., et al. 2014, A&A, 565, A39
Mahy, L., Nazé, Y., Rauw, G., et al. 2009, A&A, 502, 937
Mahy, L., Martins, F., Machado, C., Donati, J.-F., & Bouret, J.-C. 2011, A&A, 533, A9
Maíz-Apellániz, J., Walborn, N. R., Galué, H. Á., & Wei, L. H. 2004, ApJS, 151, 103
Marcolino, W. L. F., Bouret, J.-C., Martins, F., et al. 2009, A&A, 498, 837
Martins, F., & Hillier, D. J. 2012, A&A, 545, A95
Martins, F., Schaerer, D., & Hillier, D. J. 2005, A&A, 436, 1049
Martins, F., Hervé, A., Bouret, J.-C., et al. 2015, A&A, 575, A34
Mathys, G. 1989, A&AS, 81, 237
McErlean, N. D., Lennon, D. J., & Dufton, P. L. 1998, A&A, 329, 613
Mokiem, M. R., de Koter, A., Evans, C. J., et al. 2007, A&A, 465, 1003
Palate, M., Rauw, G., Koenigsberger, G., & Moreno, E. 2013, A&A, 552, A39
Petrovic, J., Langer, N., & van der Hucht, K. A. 2005, A&A, 435, 1013
Przybilla, N., Firnstein, M., Nieva, M. F., Meynet, G., & Maeder, A. 2010, A&A, 517, A38
Puls, J., Urbaneja, M. A., Venero, R., et al. 2005, A&A, 435, 669
Rivero González, J. G., Puls, J., & Najarro, F. 2011, A&A, 536, A58
Sabín-Sanjulián, C., Simón-Díaz, S., Herrero, A., et al. 2014, A&A, 564, A39
Santolaya-Rey, A. E., Puls, J., & Herrero, A. 1997, A&A, 323, 488
Schönberner, D., Herrero, A., Becker, S., et al. 1988, A&A, 197, 209
Siess, L. 2006, A&A, 448, 717
Simón-Díaz, S., & Herrero, A. 2014, A&A, 562, A135
Simón-Díaz, S., Castro, N., Herrero, A., et al. 2011, J. Phys. Conf. Ser., 328, 012021
Smith, K. C., & Howarth, I. D. 1994, A&A, 290, 868
Sota, A., Maíz Apellániz, J., Walborn, N. R., et al. 2011, ApJS, 193, 24
Sota, A., Maíz Apellániz, J., Morrell, N. I., et al. 2014, ApJS, 211, 10
Spruit, H. C. 2002, A&A, 381, 923
Talon, S., & Zahn, J.-P. 1997, A&A, 317, 749
Telting, J. H., Avila, G., Buchhave, L., et al. 2014, Astron. Nachr., 335, 41
Tetzlaff, N., Neuhäuser, R., & Hohle, M. M. 2011, MNRAS, 410, 190
van Rensbergen, W., Vanbeveren, D., & De Loore, C. 1996, A&A, 305, 825
Villamariz, M. R., & Herrero, A. 2000, A&A, 357, 597
Villamariz, M. R., & Herrero, A. 2005, A&A, 442, 263
Villamariz, M. R., Herrero, A., Becker, S. R., & Butler, K. 2002, A&A, 388, 940
Wade, G. A., Neiner, C., Alecian, E., et al. 2015, MNRAS, submitted
Walborn, N. R. 1970, ApJ, 161, L149
Walborn, N. R. 1971, ApJ, 164, L67
Walborn, N. R. 1976, ApJ, 205, 419
Walborn, N. R., Morrell, N. I., Howarth, I. D., et al. 2004, ApJ, 608, 1028
Walborn, N. R., Sota, A., Maíz Apellániz, J., et al. 2010, ApJ, 711, L143
Walborn, N. R., Maíz Apellániz, J., Sota, A., et al. 2011, AJ, 142, 150
Wellstein, S., Langer, N., & Braun, H. 2001, A&A, 369, 939
Williams, S. J., Gies, D. R., Matson, R. A., & Huang, W. 2009, ApJ, 696, L137

Pages 13 to 16 are available in the electronic edition of the journal at http://www.aanda.org

Appendix A: Additional observational information

Table A.1 provides information on the spectra used to investigate spectral variability and binarity in the ON stars sample. The spectra are shown in Fig. 11.

Table A.1. Spectroscopic data used to study variability.

Star	Date of observation	Instrument	Status
HD 12323	08 Sep. 2011	N-NOT/FIES	SB1
	12 Sep. 2011	N-NOT/FIES	
	29 Oct. 2012	M-*Mercator*/HERMES	
	29 Oct. 2012	M-*Mercator*/HERMES	
	25 Dec. 2012	N-NOT/FIES	
HD 13268	12 Jan. 2011	N-NOT/FIES	variable
	26 Oct. 2012	M-*Mercator*/HERMES	
	28 Jan. 2013	N-NOT/FIES	
	29 Jan. 2013	N-NOT/FIES	
HD 14633	13 Jan. 2009	N-NOT/FIES	SB1
	10 Sep. 2011	N-NOT/FIES	
	26 Oct. 2012	M-*Mercator*/HERMES	
	23 Dec. 2012	N-NOT/FIES	
HD 48279	14 Jan. 2011	N-NOT/FIES	constant
	24 Dec. 2012	N-NOT/FIES	
	25 Dec. 2012	N-NOT/FIES	
HD 91651	04 Apr. 2009	ESO2.2/FEROS	variable
	11 Feb. 2011	ESO2.2/FEROS	
	20 Mar. 2011	ESO2.2/FEROS	
	14 May 2011	ESO2.2/FEROS	
	15 May 2011	ESO2.2/FEROS	
	16 May 2011	ESO2.2/FEROS	
HD 102415	12 May 2008	ESO2.2/FEROS	variable
	16 May 2011	ESO2.2/FEROS	
	17 May 2011	ESO2.2/FEROS	
HD 117490	12 May 2008	ESO2.2/FEROS	variable
	13 May 2011	ESO2.2/FEROS	
	20 Mar. 2011	ESO2.2/FEROS	
	21 Mar. 2011	ESO2.2/FEROS	
	14 May 2011	ESO2.2/FEROS	
	15 May 2011	ESO2.2/FEROS	
HD 123008	13 May 2008	ESO2.2/FEROS	variable
	16 May 2011	ESO2.2/FEROS	
HD 191423	29 Aug. 2011	N-NOT/FIES	constant
	11 Sep. 2011	N-NOT/FIES	
HD 201345	09 Sep. 2010	N-NOT/FIES	constant
	17 Jun. 2011	M-*Mercator*/HERMES	
	10 Sep. 2011	N-NOT/FIES	
	25 Dec. 2012	N-NOT/FIES	

Appendix B: Best fits to the observed spectra

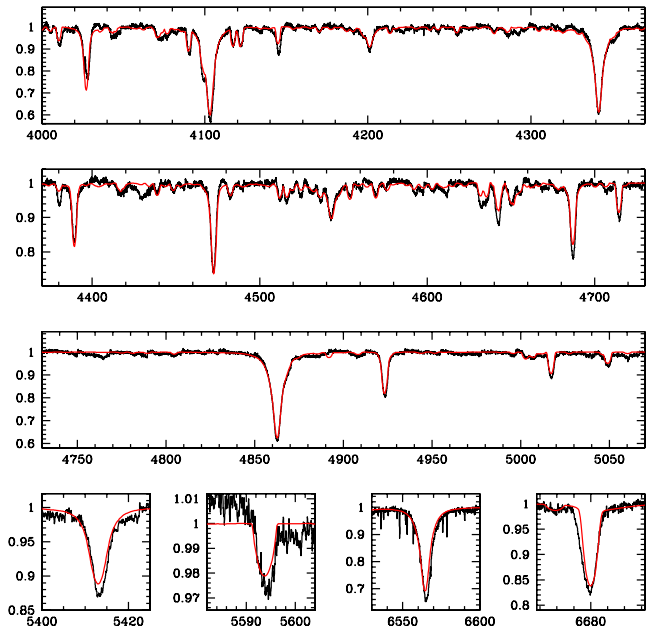

Fig. B.1. Best fit (red) of the observed spectrum (black) of HD 12323.

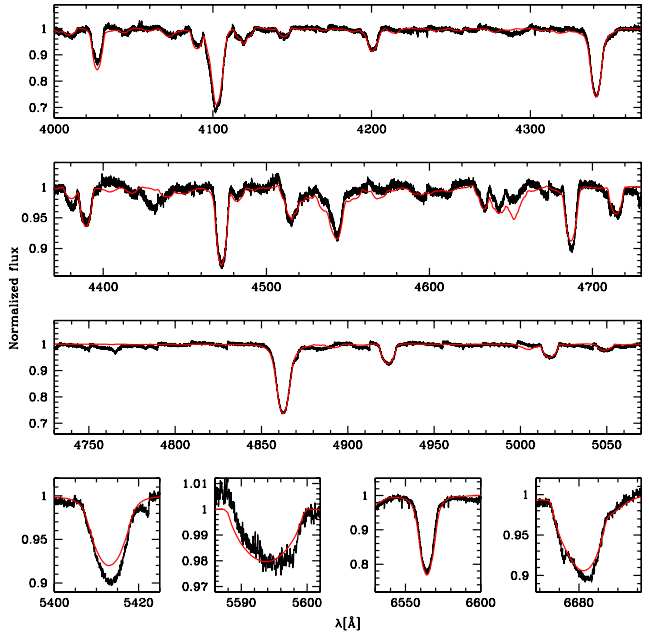

Fig. B.2. Best fit (red) of the observed spectrum (black) of HD 13268.

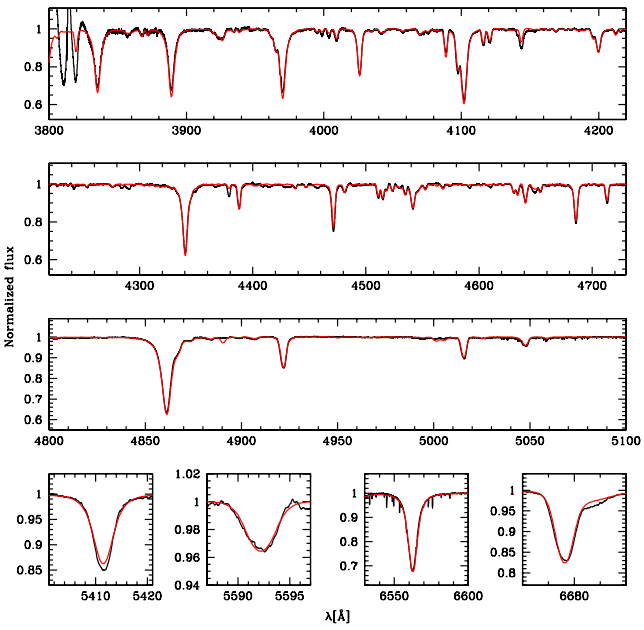

Fig. B.3. Best fit (red) of the observed spectrum (black) of HD 14633.

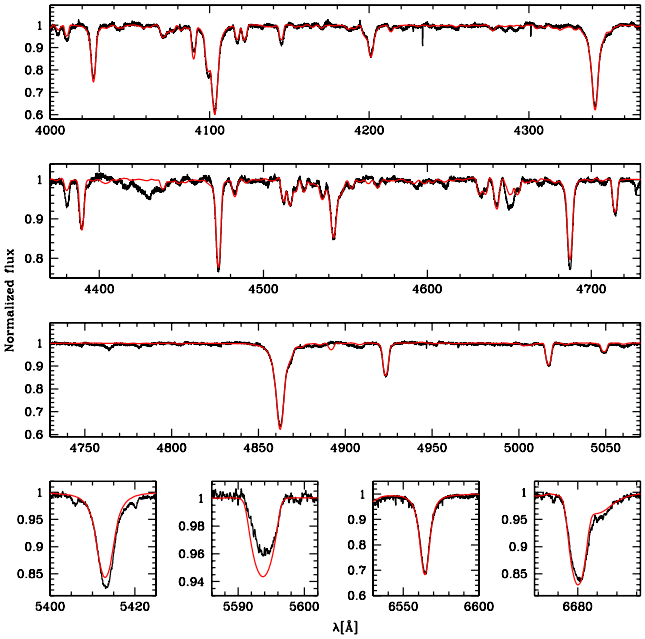

Fig. B.4. Best fit (red) of the observed spectrum (black) of HD 48279.

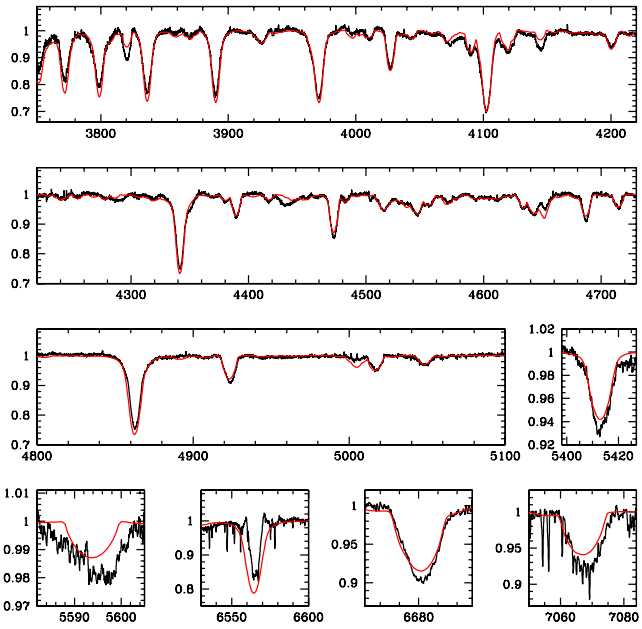

Fig. B.5. Best fit (red) of the observed spectrum (black) of HD 91651.

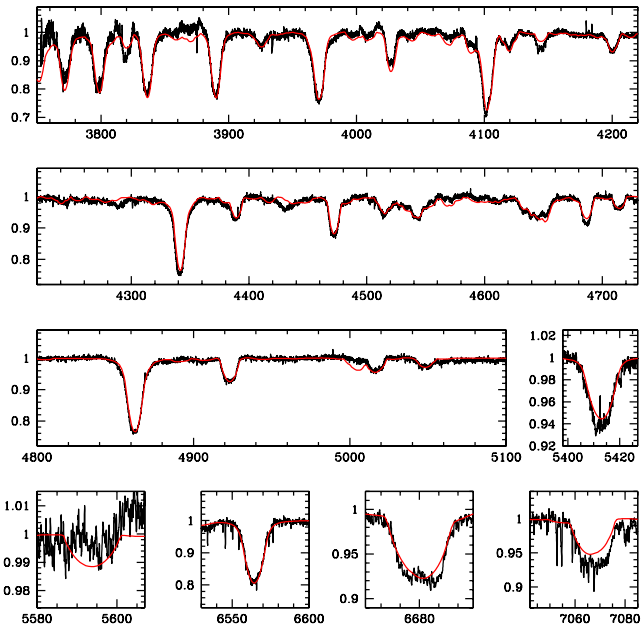

Fig. B.6. Best fit (red) of the observed spectrum (black) of HD 102415.

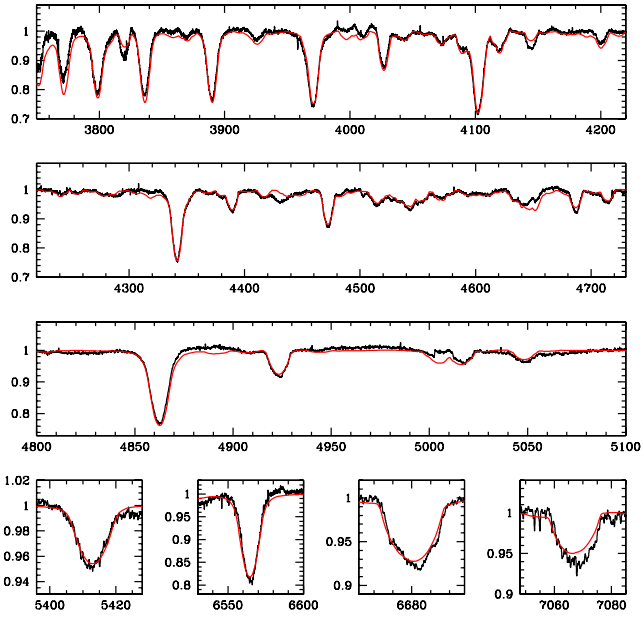

Fig. B.7. Best fit (red) of the observed spectrum (black) of HD 117490.

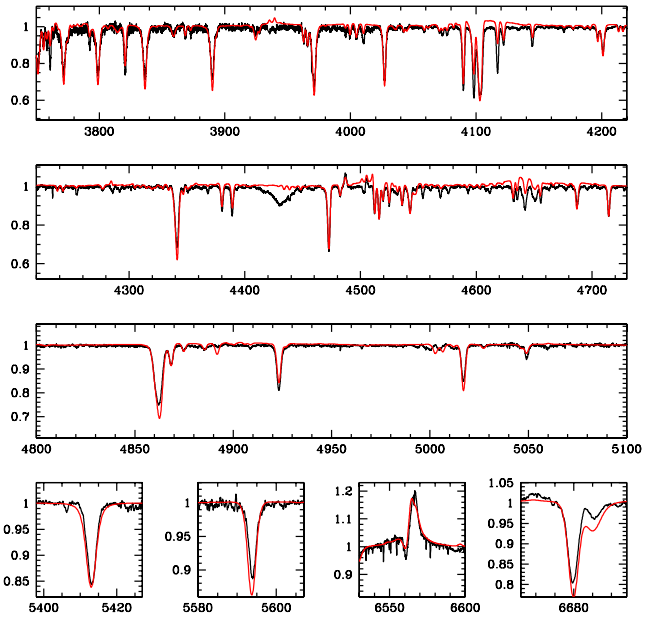

Fig. B.8. Best fit (red) of the observed spectrum (black) of HD 123008.

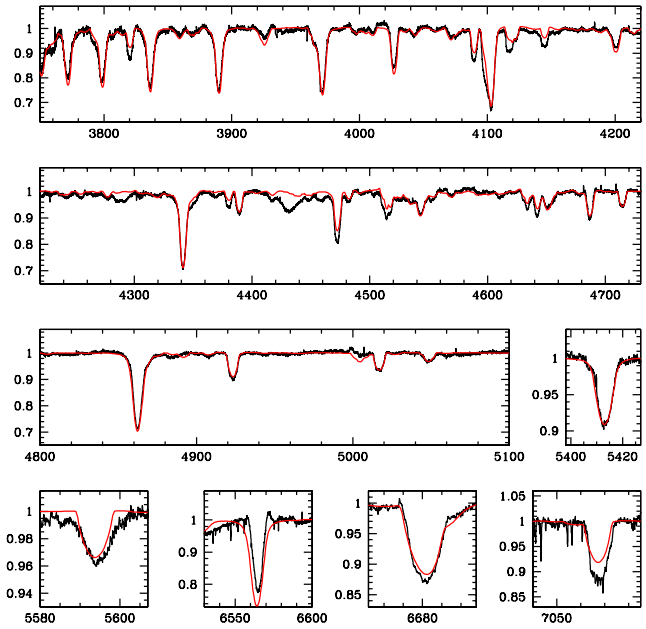

Fig. B.9. Best fit (red) of the observed spectrum (black) of HD 150574.

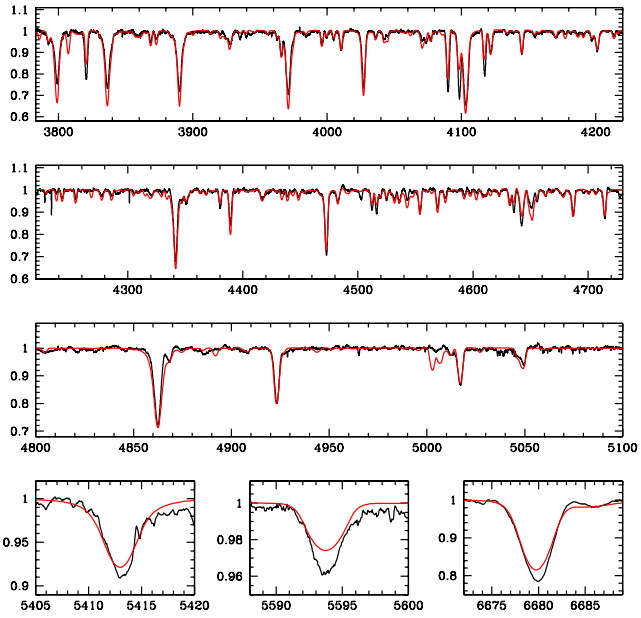

Fig. B.11. Best fit (red) of the observed spectrum (black) of HD 191781.

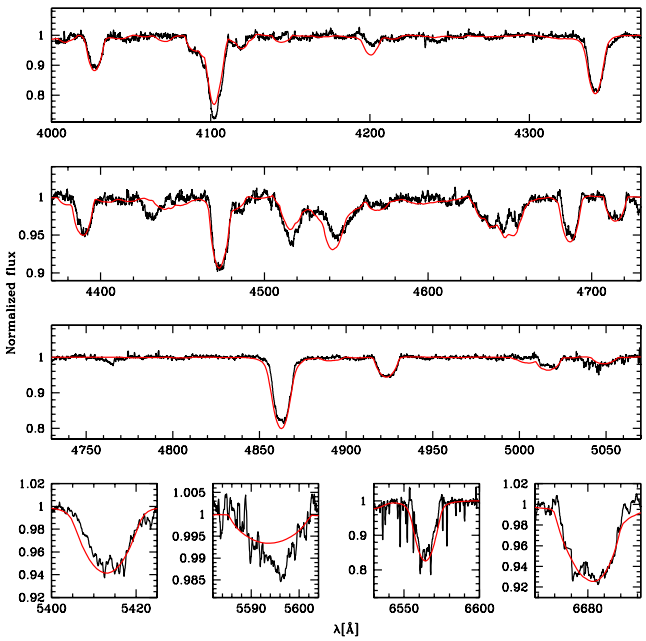

Fig. B.10. Best fit (red) of the observed spectrum (black) of HD 191423.

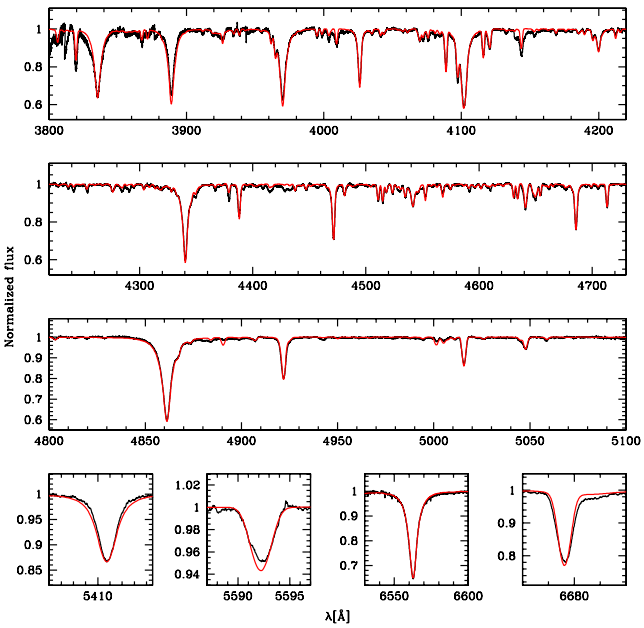

Fig. B.12. Best fit (red) of the observed spectrum (black) of HD 201345.